Nanoscale

RSC Publishing

PAPER

View Article Online
View Journal | View Issue

Published on 04 March 2013. Downloaded by National Chiao Tung University on 28/04/2014 02:04:22.

Cite this: *Nanoscale*, 2013, **5**, 3841

Enhanced broadband and omnidirectional performance of Cu(In,Ga)Se_2 solar cells with ZnO functional nanotree arrays

Ming-Yang Hsieh,[a] Shou-Yi Kuo,*[a] Hau-Vei Han,[b] Jui-Fu Yang,[ac] Yu-Kuang Liao,[d] Fang-I Lai*[ce] and Hao-Chung Kuo*[b]

Received 13th December 2012
Accepted 22nd February 2013

DOI: 10.1039/c3nr34079a

www.rsc.org/nanoscale

An effective approach is demonstrated for enhancing photoelectric conversion of Cu(In,Ga)Se_2 (CIGS) solar cells with three-dimensional ZnO nanotree arrays. Under a simulated one-sun condition, cells with ZnO nanotree arrays enhance the short-circuit current density by 10.62%. The omnidirectional anti-reflection of CIGS solar cells with various ZnO nanostructures is also investigated. The solar-spectrum weighted reflectance is approximately less than 5% for incident angles of up to 60° and for the wavelengths primarily from 400 nm to 1000 nm. This enhancement in light harvesting is attributable to the gradual refractive index profile between the ZnO nanostructures and air.

Introduction

Anti-reflection (AR) layers have frequently been applied to the surface of optoelectronic devices to reduce light reflection and increase light transmission within a specific wavelength range.[1,2] Conventional techniques use single-layer and multi-layer thin-film AR coatings, although they have some disadvantages in the thin-film stacks such as material selection, thermal expansion mismatch, and interfacial instability.[3] Since the corneas of nocturnal-moth eyes were observed in 1967 by Bernhard,[4] the surface-relief arrays have been considered an alternative to thin-film coatings. The subwavelength structures produce a gradient refractive index profile between the material (refractive index > 1) and air (refractive index = 1) to reduce Fresnel reflection and also provide a more effective thermal stability and durability than surface coatings because only one material is used.[5–7] Furthermore, the subwavelength structures have a period sufficiently smaller than the wavelength of light, and they satisfy the zeroth-order diffraction condition and suppress all higher orders of diffraction.

Solar cells have received significant attention as a potential renewable energy source. Their structures can be categorized as bulk or thin-film devices. The thin-film materials include Cu(In,Ga)Se_2 (CIGS), amorphous silicon, and CdTe.[8,9] Among these solar materials, CIGS has the greatest potential as the next generation of photovoltaic devices because CIGS solar cells have significant potential as a source of low-cost, high-efficiency solar electricity with the production efficiency greater than 20.3%.[10–12] Investigating the AR layers with subwavelength structures is an accurate technique for improving the conversion efficiency.[13,14]

Zinc oxide (ZnO) is a wide direct band gap (3.37 eV) semiconductor with a high exciton binding energy (60 meV) and excellent chemical and thermal stability. It has received considerable attention for its applications in numerous optoelectronic devices.[15–17] It is noteworthy that the reduction of absorption within the AR layer decreases the optical loss in the visible region in solar cells. Consequently, various ZnO nanostructure configurations have been reported recently, including nanowires,[18] nanorods,[19] nanotubes,[20] and nanobelts.[21] In the past few years, the fabrication processes such as electron beam lithography and dry etching have been widely used to fabricate different AR nanostructures.[22–24] However, they are not suitable for mass production of nanostructures on large-area solar cells and the process-induced surface recombination defects will decrease the device performance. Consequently, the nanostructures fabricated by using bottom-up grown methods have been developed, such as molecular beam epitaxy,[25] vapor–liquid–solid[26] growth and chemical vapor deposition.[27] In the bottom-up grown methods, the hydrothermal method is a promising method to grow ZnO nanorod arrays, because of its relatively simple fabrication and capacity for growth over large areas, low temperature, and cost efficiency. Moreover, the ZnO

[a]*Department of Electronic Engineering, Chang Gung University, 259 Wen-Hwa 1st Road, Kwei-Shan, Taoyuan 333, Taiwan. E-mail: sykuo@mail.cgu.edu.tw; Fax: +886-3-2118507; Tel: +886-3-2118800 ext. 3744*

[b]*Institute of Electro-Optical Engineering, National Chiao Tung University, 1001 University Road, Hsinchu, 300, Taiwan. E-mail: hckuo@faculty.nctu.edu.tw; Fax: +886-3-5735601; Tel: +886-3-571-2121 ext. 56304*

[c]*Department of Photonics Engineering, Yuan-Ze University, 135 Yuan-Tung Road, Chung-Li, 32003, Taiwan. E-mail: filai@saturn.yzu.edu.tw; Fax: +886-3-4514281; Tel: +886-3-4638800 ext. 7516*

[d]*Department of Electrophysics, National Chiao Tung University, Hsinchu 300, Taiwan*

[e]*Advanced Optoelectronic Technology Center, National Cheng Kung University, Tainan 701, Taiwan*

Published on 04 March 2013. Downloaded by National Chiao Tung University on 28/04/2014 02:04:22.

nanorod arrays can grow on any surface of a device by a hydrothermal method. Therefore, fabricating the ZnO nanorod structure as an AR layer was a great method.

To our knowledge, there are few studies that have discussed the characteristics of chalcopyrite solar cells with AR nanostructures. Additionally, the angle-resolved spectral reflectance of AR nanostructures had yet been studied for chalcopyrite solar cells. This study examines a hydrothermal method for growing ZnO nanostructures for the AR layer on the surface of CIGS solar cells. We experimentally investigated the optical properties of two types of nanostructures: nanorod and nanotree. By fabricating the different nanostructures, the varied profiles of the effective refractive index can be obtained. These results of CIGS solar cells with both AR nanostructures were compared with the bare one. The critical features of the AR coatings, such as broadband and omnidirectional properties, have been examined by measuring the angular reflectance. Owing to the enhanced antireflective properties, the power conversion efficiency of the CIGS solar cell with the ZnO nanostructures can be effectively improved as compared to a bare solar cell.

Experimental section

The fabrication process for the CIGS solar cell with an Al-doped ZnO (AZO)/i-ZnO/CdS/CIGS/Mo/soda-lime glass substrate structure shown in Fig. 1(a) is as follows: Deposition of the 0.9 to 1.1 μm Mo layer back electrode is performed using a DC magnetron sputtering system. The 2 μm CIGS absorber layer was grown using a co-evaporation technique. The 50 to 60 nm CdS layer was deposited using a chemical bath deposition (CBD) technique. The 50 to 60 nm i-ZnO layer and the 600 to 800 nm AZO layer were deposited using radio frequency (RF) magnetron sputtering. Finally, the Al grid is deposited using thermal evaporation as a top electrode.

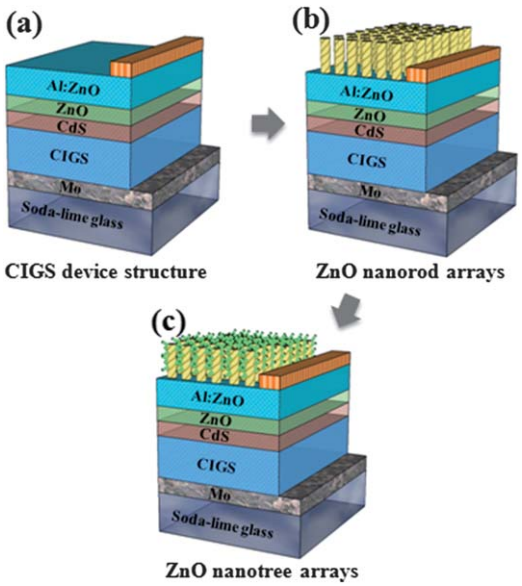

Fig. 1 Schematic process for fabricating a vertically aligned ZnO structure on the CIGS solar cell. (a) CIGS device structure, (b) ZnO nanorod arrays, and (c) ZnO nanotree.

ZnO nanostructures are grown hydrothermally to fabricate the subwavelength ZnO nanostructure on the CIGS solar cell surface. First, the transparent AZO conductive oxide layer is used as a seed layer for ZnO nanorod array growth. The aqueous solution for growing the ZnO nanorod is prepared by mixing the same concentration of 0.01 M zinc nitrate hexahydrate ($Zn(NO_3)_26H_2O$, Aldrich) and 0.01 M hexamethylenetetramine ($C_6H_{12}N_4$, HMT, Aldrich). The hydrothermal chemical reactions for the ZnO structures are as follows:

$$C_6H_{12}N_4 + 6H_2O \rightarrow 6HCHO + 4NH_3 \quad (1)$$

$$NH_3 + H_2O \rightarrow NH_4^+ + OH^- \quad (2)$$

$$Zn^{2+} + 2OH^- \rightarrow Zn(OH)_2 \quad (3)$$

$$Zn(OH)_2 \rightarrow (\text{heat}) \rightarrow ZnO + H_2O \quad (4)$$

After mixing the two aqueous solutions, the solar cells are immersed in the solution at 90 °C for 9 h. D.I. water is used to clean the cell after the nanorod growth process is completed before it is heated to 60 °C in air for 1 h. A 100 nm AZO layer is then deposited using RF magnetron sputtering as a seed layer for ZnO nanobranches array growth. Afterward the hydrothermal process is repeated until the length of branches meets the requirement.

The deposited profile and surface morphologies of the fabricated ZnO structures on cells are observed using field emission scanning electron microscopy (FESEM, Hitachi S-4700I). Crystalline ZnO structures are analyzed using X-ray diffraction (XRD). The angle-dependent reflectance is measured using a UV-VIS-NIR spectrophotometer for wavelengths between 400 and 1000 nm with incident angles between −60° and 60°. The CIGS solar cell performance is measured at room temperature using a solar simulator at an irradiation intensity of 1000 W m^{-2} (AM1.5G).

Results and discussion

The CIGS solar cell surface morphology with and without vertically aligned ZnO nanostructures is shown in Fig. 2. Fig. 2(a), (c) and (e) show the cross-sectional scanning electron microscopy (SEM) images, and Fig. 2(b), (d) and (f) show the top view SEM images. The images of the AZO top layer surface (Fig. 2(a) and (b)) show uniform seed distribution. Fig. 2(c) and (d) show the ZnO nanorods grown on a uniform AZO film from the first hydrothermal process. The diameter of the ZnO nanorods range from 80 to 130 nm, and the mean height is approximately 1 μm. Fig. 2(e) and (f) show the ZnO nanobranches subsequently grown on the nanorod arrays. The diameter of the ZnO nanobranches ranges from 40 to 50 nm, and the mean height is approximately 400 nm. The diameters of the ZnO nanobranches are relatively small than those of the nanorods, originating from the different grain sizes of the seed layer for growing rods and branches. Fig. 2(f) shows that the ZnO nanobranches are not perpendicular but oblique to the columnar surface of the nanorods. According to previous literature, in order to achieve high transmittance and low

 This journal is © The Royal Society of Chemistry 2013

Published on 04 March 2013. Downloaded by National Chiao Tung University on 28/04/2014 02:04:22.

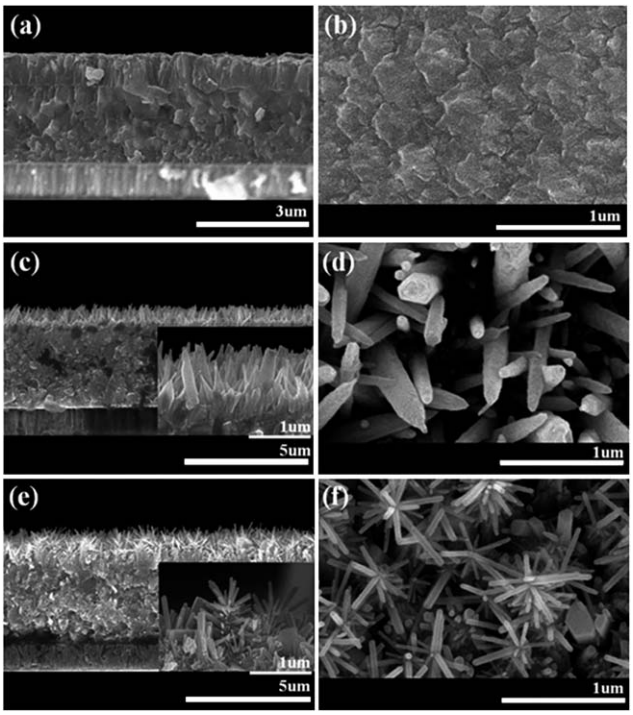

Fig. 2 SEM images of the ZnO structures grown on flat CIGS solar cells (left: cross-section, right: top view): a CIGS solar cell (a and b) with a flat surface (c and d) with ZnO nanorods, and (e and f) with ZnO nanotrees.

reflectance of efficient AR structures, the shape of the structure should be fulfilled by the following conditions:[28–30]

$$h \geq 0.4\lambda_{\text{longest}}, \tag{5}$$

$$\Lambda < \frac{\lambda_{\text{shortest}}}{n}, \tag{6}$$

where h is the height of the ZnO nanostructure, λ_{longest} and $\lambda_{\text{shortest}}$ are the longest and shortest operational wavelengths respectively, Λ is the center-to-center spacing of the ZnO nanostructures, and n is the refractive index of the material. In this paper, the operational wavelengths of the CIGS solar cell were set at wavelengths from 400 to 1000 nm that were excellently absorbed in a CIGS solar cell. Therefore, according to eqn (5), the height of the nanostructures should be higher than 400 nm, and the diameter of the nanostructures should be smaller than 200 nm according to eqn (6). In this work, the ZnO tree-like nanostructures grown on the CIGS solar cell fulfilled the theoretical requirements and achieved efficient AR structures as shown in Fig. 2.

In order to more clearly investigate the crystal of ZnO nanostructures, the ZnO nanorod and nanotree structures grown on the AZO film are also investigated. Fig. 3(a) shows an XRD pattern of the ZnO nanorod and nanotree grown on the AZO film. The strong diffraction peak at 34.4° on the AZO film and AZO film with nanorods corresponds to the (002) plane along the *c*-axis. The three peaks at 34.4°, 36.3°, and 72.5° in the nanotree sample represent the (002), (101), and (004) ZnO crystal planes. It is assigned to a pure wurtzite ZnO phase as referred to the JCPDS file 36-1451. Therefore, XRD analysis

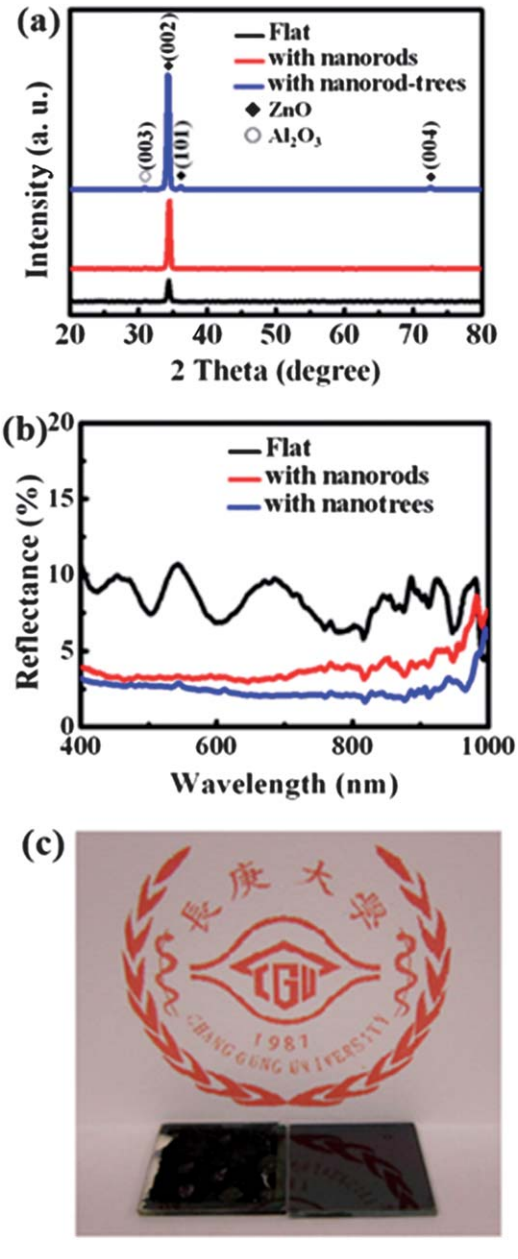

Fig. 3 (a) X-ray diffraction patterns of ZnO nanotrees grown on the AZO film. (b) Reflectance measurements of ZnO nanorods and nanotrees grown on CIGS solar cells compared with a bare one. (c) Images of (right) a CIGS solar cell with ZnO nanotree arrays and (left) a bare CIGS solar cell.

shows that perpendicularly oriented ZnO crystals form the CIGS solar cell surface, as well as other crystal planes. Additionally, the XRD analysis corresponds to the SEM images.

To investigate the AR characteristics of the nanostructures over the broad range of wavelengths, Fig. 3(b) shows the reflectance of the CIGS solar cells with ZnO nanorod arrays and ZnO nanotree arrays compared with a bare CIGS solar cell. The reflectance is measured using an integrating sphere at the normal incidence of light. The result indicates that the ZnO nanostructures reduce the reflectance compared to that of a bare CIGS cell. The mean reflectance of the bare CIGS cell is approximately 8.27%, whereas the mean reflectance of the CIGS

Published on 04 March 2013. Downloaded by National Chiao Tung University on 28/04/2014 02:04:22.

cell with ZnO nanorods grown on the surface decreases to 3.84%. Finally, the mean reflectance decreases to 2.51% when the nanotrees are grown on the surface. ZnO structures grown on the CIGS cell surface cause the amplitude of the interference fringe in the visible range (400 to 800 nm) to fade. Moreover, the reflectance decreases at every wavelength. Therefore, this study proposes that the ZnO nanostructures are suitable for wavelength-independent AR coatings for CIGS solar cells.

Fig. 3(c) shows the images from (right) a bare CIGS solar cell and (left) that with nanotrees. The reflection characteristics of these AR-coated cells are imaged using the reflection of a school badge on paper. The grown ZnO nanotrees degraded the brightness of the reflection characteristics, which is in agreement with the results shown in Fig. 3(b).

The incident angle-dependent optical properties are crucial for solar cells because of the movement of the sun. To evaluate the performance of omnidirectional AR characteristics, Fig. 4(a)–(c) show the measured angle-dependent reflectance of CIGS solar cells with flat (bare cell), nanorod, and nanotree layers, respectively. The angle-dependent mappings were conducted on the CIGS solar cells at wavelengths from 400 to 1000 nm. The reflectance spectra are measured at incident angles between −60° and 60°. The red and blue colors in the color bar represent the low to high reflectance. These angle-dependent mappings show that the lowest reflectance is that of the CIGS solar cell with the nanotree structures. Therefore, the nanotree structure successfully reduces the broadband reflectivity at the normal incidence and reduces reflectance for incident angles between −60° and 60°. The variation in reflectance behavior is attributable to the gradual refractive index from the air to the cell surface and has been studied by several scholars.[31,32] To compare the angle-dependence of solar power harvesting, an AM1.5G solar-spectrum weighted reflectance was calculated using the following equation to express the antireflective power of the nanostructures and plotted in Fig. 4(d).

$$R_{\text{Weighted}} = \frac{\int_{400\text{ nm}}^{1000\text{ nm}} R(\lambda) I_{\text{AM1.5G}}(\lambda)\,\mathrm{d}\lambda}{\int_{400\text{ nm}}^{1000\text{ nm}} I_{\text{AM1.5G}}(\lambda)\,\mathrm{d}\lambda} \quad (7)$$

where $R(\lambda)$ is the measured reflectivity shown in Fig. 4(a)–(c), and $I_{\text{AM1.5G}}$ is the photon flux density of the AM1.5G solar spectrum. As shown in Fig. 4(d), the weighted reflectance of the nanotree cell shows an excellent decrease at every wavelength compared to the bare and with nanorod cells. It is noteworthy at an incident angle of 60°, the weighted reflectance of the nanotree cell is approximately less than 5%, while the bare cell is 13%. This observation reveals that the angle-dependence for AR coating of the ZnO nanotree is more suitable for CIGS solar cells than others. Besides, in order to maximize the efficiency of light collected, the sunlight tracking system is also generally used to minimize the angle of incidence between the incoming light and a solar cell surface. Taking the ZnO nanotree as an AR layer on a solar cell, they not only inhibit the broadband reflectivity at normal incidence but also can reduce optical reflection for a large incidence of light, promising a superior photocurrent generation over an entire day. Consequently, growing a ZnO nanotree structure as an AR layer is a potential candidate for saving the cost of a sunlight tracking system.

In the past, theoretical papers approximate sub-wavelength structures as effective multilayer stacks and use the effective medium theory (EMT) to describe the optical properties, in which the refractive index increases gradually from air to the AZO layer.[33–35] Therefore, the EMT adopted to explain the Fresnel reflection can be efficiently suppressed by the ZnO nanostructures. The geometric features can be observed in the SEM images, which provide the estimative size of different ZnO nanostructures, as shown in Fig. 2. While the incident light is reflected from the surface, the wavelengths of reflection will be reduced through destructive interferences, where the phases of the waves will cancel one another partially or wholly. Particularly, the reflectance may decrease at the surface with ZnO nanostructures, owing to the enhanced destructive interferences. In addition, from the previous research on the effective multilayer thin-film AR coatings, the reflectance of a multilayer was lower than that of a single layer and the bandwidth may become broader.[36] The phenomenon originates from the fact that the multilayer thin-film AR coatings have a smoother grading in the refractive index. In this work, the ZnO nanorod structure can be treated as an effective single layer, and the ZnO nanotree structure as an effective double layer. The effective refractive index (n_{eff}) of the grown ZnO nanostructure can be calculated using the following weighting formula:[37]

$$n_{\text{eff}} = \left[{n_{\text{ZnO}}}^2 \times f + {n_{\text{air}}}^2 (1-f)\right]^{\frac{1}{2}} \quad (8)$$

where f is the filling factor by ZnO nanostructures, and n_{ZnO} and n_{air} are refractive indexes of ZnO and air, respectively. In the calculations, the refractive index of ZnO is about 2.1, and the filling factor is estimated from the SEM images. For the ZnO

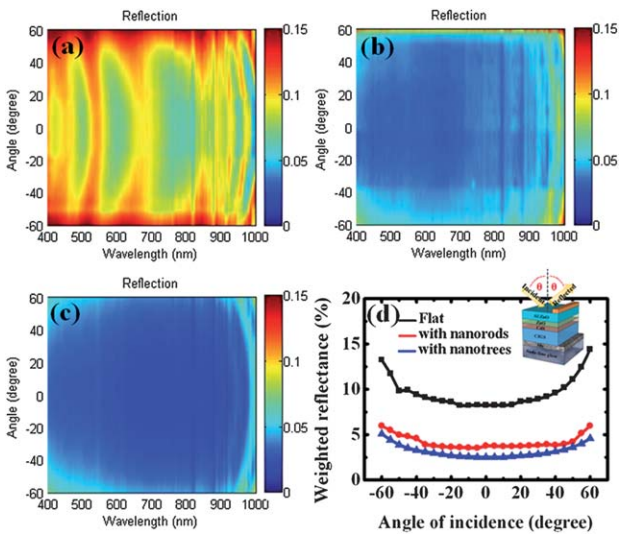

Fig. 4 The measured angular reflectance spectra for a solar cell with (a) bare, (b) with a rod structure, (c) with a tree structure and (d) the weighted reflectance of all cells, calculated by the measured angular reflectance spectra shown in (a)–(c). The inset in (d) is a schematic illustration of the angle dependence between incident and reflected light.

 This journal is © The Royal Society of Chemistry 2013

Published on 04 March 2013. Downloaded by National Chiao Tung University on 28/04/2014 02:04:22.

nanorod structure, the filling factor was 0.22 and the value of n_{eff} was calculated as 1.32 for the height of a 1 μm ZnO nanorod. For the ZnO nanotree structure, the filling factor was 0.49 (0.154) at the stem (branch) of the tree structure. Therefore, the effective n_{eff} of the stem and branch were calculated as 1.64 and 1.23 respectively. The calculated refractive index profiles are plotted in Fig. 5. As shown in Fig. 5, the ZnO nanorod and tree structures exhibit equivalent two-step and three-step variations of refractive index profiles, respectively. These characteristics in nanostructures with the rod and tree are similar to those shown in the effective single layer and double layer. Therefore, the solar cell with a nanotree structure was expected to possess the lower reflection due to the smoother grading in the effective refractive index profile than the bare CIGS cells and those with nanorod structure.

Fig. 6 shows the CIGS solar cells with ZnO nanorod arrays and ZnO nanotree arrays in the AM1.5G light spectrum compared to a bare CIGS solar cell. The parameters are shown in Table 1. The bare CIGS solar cell and the cell with ZnO nanotree arrays have conversion efficiencies (η) of 9.13% and 10.06% with an approximate open-circuit voltage (V_{oc}) of 0.67 V,

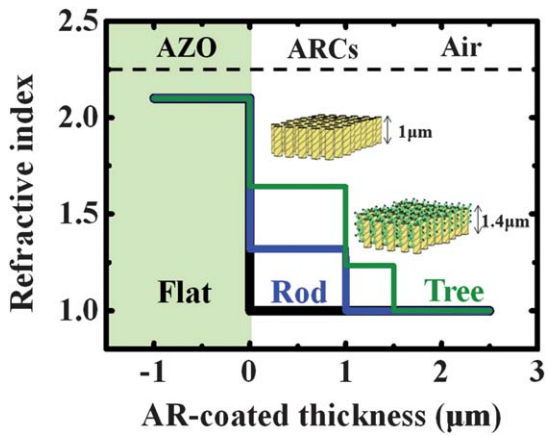

Fig. 5 Schematic illustration of the refractive index profiles of different ZnO nanostructures AR-coated on CIGS solar cells with varying AR-coated thickness.

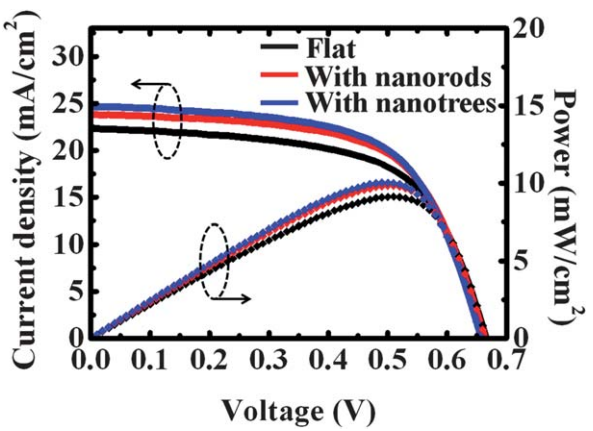

Fig. 6 Light current density–voltage (*J–V*) characteristics of different ZnO nanostructures AR-coated on CIGS solar cells.

Table 1 Photovoltaic parameters of different ZnO nanostructures AR-coated on CIGS solar cells

Samples	V_{oc} (V)	J_{sc} (mA cm^{-2})	FF	η(%)
Flat	0.67	22.32	0.61	9.13
Rod	0.67	23.84	0.616	9.84
Rod-tree	0.66	24.69	0.615	10.02

J_{sc} of 22.32 mA cm^{-2} and 24.69 mA cm^{-2}, and a fill factor (FF) of 0.61 and 0.615, respectively. Thus, the photovoltaic efficiency is enhanced because J_{sc} of the CIGS solar cell with the ZnO nanotree arrays is greater than the bare cell. The extra gain (G_{jsc}) in photocurrent is calculated by

$$G_{jsc} = \frac{\Delta J_{sc}}{J_{sc}} = \frac{J_{sc}(\text{with ARc}) - J_{sc}(\text{without ARc})}{J_{sc}(\text{without ARc})} \quad (9)$$

Because of the enhanced AR effects, the extra gain in photocurrent G_{jsc} for the CIGS solar cells with ZnO nanorod arrays and ZnO nanotree arrays are 6.81% and 10.62%, respectively. Moreover, the ZnO nanotree AR effect enhanced the conversion efficiency to 10.02% because of the increase in short-circuit current. Additionally, the shunt resistances and series resistances in these solar cells were approximately 500 and 5 ohm cm^2, calculated from the current density–voltage curves. This result means that the electricity of the CIGS solar cell with ZnO nanostructures grown by the hydrothermal process was less affected. Consequently, the ZnO nanorod structure is expected to be a suitable alternative AR layer for electro-optical devices in the future.

Conclusions

In conclusion, a CIGS solar cell with nanotree arrays is shown using a hydrothermal deposition method. The ZnO nanotree arrays possess superior AR properties across a broad spectral range and angles of incidence. Because the structures can reduce surface Fresnel reflection, the mean reflectance of the bare CIGS solar cell and those with the ZnO nanotree arrays are 8.24% and 3.59%, respectively. Moreover, the ZnO nanotree AR effect enhances the conversion efficiency to 10.02% because of the increase in short-circuit current. Therefore, because of the cost-efficient and low-temperature fabrication process, this study proposes that the discussed nanotree arrays are a suitable alternative AR layer for other electro-optical devices.

Acknowledgements

This work was also supported by the Green Technology Research Center of Chang Gung University and the National Science Council (NSC) of Taiwan under contract nos NSC101-2112-M-182-003-MY3 and NSC101-3113-E-182-001-CC2.

Notes and references

1 B. S. Richards, *Prog. Photovolt: Res. Appl.*, 2004, **12**, 253–281.
2 V. M. Aroutiounian, K. Martirosyan and P. Soukiassian, *J. Phys. D: Appl. Phys.*, 2006, **39**, 1623–1625.

Published on 04 March 2013. Downloaded by National Chiao Tung University on 28/04/2014 02:04:22.

3 P. Lalanne and G. M. Morris, *Proc. SPIE*, 1996, **2776**, 300.
4 C. G. Bernhard, *Endeavour*, 1967, **26**, 79–84.
5 P. Lalanne and G. M. Morris, *Nanotechnology*, 1997, **8**, 53–56.
6 M. Y. Chiu, C. H. Chang, M. A. Tsai, F. Y. Chang and P. Yu, *Opt. Express*, 2010, **18**, A308–A313.
7 J. W. Leem, D. H. Joo and J. S. Yu, *Sol. Energy Mater. Sol. Cells*, 2011, **95**, 2221–2227.
8 S. Muthmann and A. Gordijn, *Sol. Energy Mater. Sol. Cells*, 2011, **95**, 573–578.
9 M. Kim, S. Sohn and S. Lee, *Sol. Energy Mater. Sol. Cells*, 2011, **95**, 2295–2301.
10 P. Jackson, D. Hariskos, E. Lotter, S. Paetel, R. Wuerz, R. Menner, W. Wischmann and M. Powalla, *Prog. Photovolt: Res. Appl.*, 2011, **19**, 894–897.
11 A. Chirilă, S. Buecheler, F. Pianezzi, P. Bloesch, C. Gretener, A. R. Uhl, C. Fella, L. Kranz, J. Perrenoud, S. Seyrling, R. Verma, S. Nishiwaki, Y. E. Romanyuk, G. Bilger and A. N. Tiwari, *Nat. Mater.*, 2011, **10**, 1–5.
12 L. Zhang, Q. He, W. L. Jiang, F. F. Liu, C. J. Li and Y. Sun, *Sol. Energy Mater. Sol. Cells*, 2009, **93**, 114–118.
13 P. C. Tseng, P. Yu, H. C. Chen, Y. L. Tsai, H. W. Han, M. A. Tsai and C. H. Chang, *Sol. Energy Mater. Sol. Cells*, 2011, **95**, 2610–2615.
14 J. W. Leem and J. S. Yu, *Opt. Express*, 2012, **20**, A431–A440.
15 M. A. Martinez, J. Herrero and M. T. Gutierrez, *Sol. Energy Mater. Sol. Cells*, 1997, **45**, 75–86.
16 M. M. Islama, S. Ishizuka, A. Yamada, K. Matsubara, S. Niki, T. Sakurai and K. Akimoto, *Appl. Surf. Sci.*, 2011, **257**, 4026–4030.
17 S. Y. Kuo, K. C. Liu, F.-I. Lai, J. F. Yang, W. C. Chen, M. Y. Hsieh, H.-I. Lin and W. T. Lin, *Microelectron. Reliab.*, 2010, **50**, 730.
18 M. K. Kim, D. K. Yi and U. Paik, *Langmuir*, 2010, **26**, 7552–7554.
19 Y. H. Zheng, L. R. Zheng, Y. Y. Zhan, X. Y. Lin, Q. Zheng and K. M. Wei, *Inorg. Chem.*, 2007, **46**, 6980–6986.
20 M. S. Samuel, J. Koshy, A. Chandran and K. C. George, *Curr. Appl. Phys.*, 2011, **11**, 1094–1099.
21 J. X. Wang, C. M. L. Wu, W. S. Cheung, L. B. Luo, Z. B. He, G. D. Yuan, W. J. Zhang, C. S. Lee and S. T. Lee, *J. Phys. Chem. C*, 2010, **114**, 13157–13161.
22 P. C. Tseng, P. Yu, H. C. Chen, Y. L. Tsai, H. W. Han, M. A. Tsai, C. H. Chang and H. C. Kuo, *Sol. Energy Mater. Sol. Cells*, 2011, **95**, 2610–6215.
23 O. Gunawan, K. Wang, B. Fallahazad, Y. Zhang, E. Tutuc and S. Guha, *Prog. Photovolt: Res. Appl.*, 2011, **19**, 307–312.
24 M. Huang, C. Yang, Y. Chiou and R. Lee, *Sol. Energy Mater. Sol. Cells*, 2008, **92**, 1352–1357.
25 B. Fuhrmann, H. S. Leipner, H. Höche, L. Schubert, P. Werner and U. Gösele, *Nano Lett.*, 2005, **5**, 2524–2527.
26 M. C. Putnam, S. W. Boettcher, M. D. Kelzenberg, D. B. Turner-Evans, J. M. Spurgeon, E. L. Warren, R. M. Briggs, N. S. Lewis and H. A. Atwater, *Energy Environ. Sci.*, 2010, **8**, 1037–1041.
27 L. Tsakalakos, J. Balch, J. Fronheiser, B. A. Korevaar, O. Sulima and J. Rand, *Appl. Phys. Lett.*, 2007, **91**, 233117.
28 S. J. Wilson and M. C. Hutley, *Opt. Acta*, 1982, **29**, 993–1009.
29 W. H. Southwell, *J. Opt. Soc. Am. A*, 1991, **8**, 549–553.
30 D. H. Raguin and G. M. Morris, *Appl. Opt.*, 1993, **32**, 1154–1167.
31 N. D. Arora and J. R. Hauser, *J. Appl. Phys.*, 1982, **53**, 8839–8846.
32 B. K. Shin, T. I. Lee, J. Xiong, C. Hwang, G. Noh, J. H. Cho and J. M. Myoung, *Sol. Energy Mater. Sol. Cells*, 2011, **95**, 2650–2654.
33 M. Minot, *J. Opt. Soc. Am.*, 1977, **67**, 1046–1050.
34 W. H. Southwell, *J. Opt. Soc. Am. A*, 1991, **8**, 549–553.
35 D. H. Raguin and G. M. Morris, *Appl. Opt.*, 1993, **32**, 1154–1167.
36 U. Schulz, *Opt. Express*, 2009, **17**, 8704–8708.
37 J. Zhong, H. Chen, G. Saraf, Y. Lu, C. K. Choi, J. J. Song, D. M. Mackie and H. Shen, *Appl. Phys. Lett.*, 2007, **90**, 203515.

 This journal is © The Royal Society of Chemistry 2013